Extracellular and intracellular effects of bioactive glass nanoparticles on osteogenic differentiation of bone marrow mesenchymal stem cells and bone regeneration in zebrafish osteoporosis model

Meng, Li; Zhao, Panpan; Jiang, Yucheng; You, Jiawen; Xu, Zhiyan; Yu, Kui; Boccaccini, Aldo R.; Ma, Junqing; Zheng, Kai

Full length article

Extracellular and intracellular effects of bioactive glass nanoparticles on osteogenic differentiation of bone marrow mesenchymal stem cells and bone regeneration in zebrafish osteoporosis model

Li Meng [a,c,1], Panpan Zhao [a,c,1], Yucheng Jiang [a], Jiawen You [a], Zhiyan Xu [d], Kui Yu [e], Aldo R. Boccaccini [d], Junqing Ma [a,b,c,*], Kai Zheng [a,c,*]

[a] Jiangsu Engineering Research Center of Stomatological Translational Medicine, Nanjing Medical University, Nanjing 210029, China
[b] Department of Orthodontics, Affiliated Hospital of Stomatology, Nanjing Medical University, Nanjing 210029, China
[c] Jiangsu Key Laboratory of Oral Diseases, Nanjing Medical University, Nanjing 210029, China
[d] Institute of Biomaterials, University of Erlangen-Nuremberg, 91058 Erlangen, Germany
[e] Department of Bionanoscience, Kavli Institute of Nanoscience, Delft University of Technology, 2629 HZ Delft, the Netherlands

ARTICLE INFO

ABSTRACT

Bioactive glass nanoparticles (BGNs) are well-recognized multifunctional biomaterials for bone tissue regeneration due to their capability to stimulate various cellular processes through released biologically active ions. Understanding the correlation between BGN composition and cellular responses is key to developing clinically usable BGN-based medical devices. This study investigated the influence of CaO content of binary SiO_2-CaO BGNs (CaO ranging from 0 to 10 mol%) on osteogenic differentiation of rat bone marrow mesenchymal stem cells (rBMSCs) and *in vivo* bone regeneration in zebrafish osteoporosis model. The results showed that BGNs could promote osteogenic differentiation of rBMSCs by indirectly releasing active ions or directly interacting with rBMSCs by internalization. In both situations, BGNs of a higher CaO content could promote the osteogenic differentiation of rBMSCs to a greater extent. The internalized BGNs could activate the transcription factors RUNX2 and OSX, leading to the expression of osteogenesis-related genes. The results in the zebrafish osteoporosis model indicated that the presence of BGNs of higher CaO contents could enhance bone regeneration and rescue dexamethasone-induced osteoporosis to a greater extent. These findings demonstrate that BGNs can stimulate osteogenic differentiation of rBMSCs by releasing active ions or internalization. A higher CaO content facilitates osteogenesis and bone regeneration of zebrafish as well as relieving dexamethasone-induced osteoporosis. The zebrafish osteoporosis model can be a potent tool for evaluating the *in vivo* bone regeneration effects of bioactive materials.

Statement of significance

Bioactive glass nanoparticles (BGNs) are increasingly used as fillers of nanocomposites or as delivery platforms of active ions to regenerate bone tissue. Various studies have shown that BGNs can enhance osteogenic differentiation of bone marrow mesenchymal stem cells (BMSCs) by releasing active ions. However, the correlation between BGN composition and cellular responses and *in vivo* bone regeneration effect has still not been well investigated. Establishment of a suitable *in vivo* animal model for investigating this correlation is also challenging. The present study reports the influence of CaO content in binary SiO_2-CaO BGNs on osteogenic differentiation of BMSCs extracellularly and intracellularly. This study also demonstrates the suitability of zebrafish osteoporosis model to investigate *in vivo* bone regeneration effect of BGNs.

1. Introduction

Bioactive glass nanoparticles (BGNs) are biocompatible and biodegradable materials able to promote angiogenesis, osteogenesis, and antibacterial activity, which have been extensively applied

* Corresponding authors.
E-mail addresses: kaizheng@njmu.edu.cn (K. Zheng), jma@njmu.edu.cn (J. Ma).
[1] These authors contributed equally to this work.

as bioactive materials in hard and soft tissue regeneration [1–5]. BGNs are also characteristic of regulable morphology and particle size, and large specific surface area, consequently leading to great acellular and cellular bioactivity [1,6]. BGNs are generally applied as rigid fillers of composites to tune the physiochemical and mechanical properties of matrices [7]. BGNs as fillers can indirectly affect cellular properties by releasing active ions during degradation [8]. In addition, they can also directly interact with cells to modulate cellular activities toward enhanced cell proliferation and osteogenic differentiation [9]. Understanding direct and indirect interactions between BGNs and cells is key to developing clinically applicable BGN-based medical devices.

Chemical composition is the main determinant to the physiochemical and biological features of BGNs. Calcium (Ca) is an essential element for BGs, as it plays critical roles in biomineralization, osteogenic and hemostatic activities that are crucial properties for BG applications [10]. Binary SiO_2-CaO BGNs have attracted considerable attention in biomedical applications due to their controllable composition, uniform size and shape [11]. Moreover, a controllable degradation and Ca ion release can be achieved relatively conveniently in SiO_2-CaO BGNs compared to BGNs of complex compositions, such as 45S5 BG composition [11–13]. Previous studies have focused on synthesizing SiO_2-CaO BGNs and the effects of CaO content on acellular bioactivity and protein adsorption behavior [11,12]. However, the influence of CaO content in SiO_2-CaO BGNs on their osteogenic activity has not been particularly focused on. Given the potential applications of BGNs, it is necessary to understand how SiO_2-CaO BGNs and the CaO content influence the osteogenic activity of cells directly or indirectly.

Various cell lines, such as bone marrow mesenchymal stem cells (BMSCs) and osteoblasts, have been used to evaluate the osteogenic potential of BGNs, generating numerous *in vitro* evidence. However, the condition of *in vitro* cell models is still far away from the actual condition in which BGNs are used. Although animal models (*e.g.*, rats, rabbits) have been applied to evaluate the bone repair and regeneration capability of BG-based tissue engineering scaffolds or implants [14], cost-effective, convenient and convincing models that can reflect the actual behaviors of BGNs in bone repair processes are still highly demanded. Zebrafish (Danio rerio), a small fresh-water teleost, has been well-recognized as a valuable animal model for evaluating the biological behaviors of biomaterials, drugs and cosmetics due to its high fertility, rapid external embryonic development, genetic similarity with humans, small size and low cost of animal husbandry [15]. Zebrafish is a vertebrate showing strong similarities in skeletal physiology to mammals. In addition, the molecular basis and key regulators of bone formation between zebrafish and mammals are highly similar [16,17]. The bone development of zebrafish also originates from mesenchymal cells [18]. Considering these benefits, zebrafish is increasingly used as models in biomedical skeletal research [15,19]. Particularly, diseased skeletal models can be created using zebrafish, such as osteoporosis zebrafish models.

Osteoporosis is a systemic skeletal disorder characterized by micro-architectural deterioration of bone tissue and loss of bone mass, resulting in bone fragility and increased fracture risk [20,21]. BGs have been considered to treat osteoporosis due to their capability to promote osteogenesis [22]. Osteoporotic bone defects of rats and rabbits have been applied to evaluate the effects of BG-based materials on treating osteoporosis [17,23]. However, there are still limitations in these animal models, such as the high cost of acquisition and maintenance, ethical dilemmas and long periodicity [24]. Alternatively, zebrafish models have advantages over these animal models in evaluating the performance of biomaterials in osteoporosis therapy, for example, a high number of offspring, a short generation time, external development and translucent early-life stages [25]. Thus, the zebrafish osteoporosis model is expected

Table 1

Chemical compositions of BGNs and the amount of calcium nitrate tetrahydrate added in the synthesis.

	Chemical composition (mol%)		CaN added (g)
	SiO_2	CaO	
100S	100	0	0
99S	99	1	0.127
95S	95	5	0.668
90S	90	10	1.409

to be a potent tool for evaluating the therapeutic effects of BGs on osteoporosis. However, this beneficial model has not yet been used to assess the osteogenic potential of BGNs, though the zebrafish model has been applied to assess the osteogenic activity of micro-sized BGs [26] and bioactive ions [27] as well as the angiogenesis of Cu-containing mesoporous bioactive glasses (MBGs) [28].

In this study, we investigated the influence of CaO content of binary SiO_2-CaO BGNs (CaO concentrations ranging from 0 to 10 mol%) on *in vitro* osteoblastic differentiation of rat bone marrow mesenchymal stem cells (rBMSCs) and *in vivo* bone regeneration in a zebrafish osteoporosis model. Particularly, we compared two culture approaches, *i.e.*, direct exposure of BGNs to rBMSCs and indirect exposure (ionic dissolution products) to rBMSCs, to understand the osteogenic potential of BGNs in different application scenarios (delivery platforms of ions and composite fillers, respectively). Our results revealed that increased CaO content could promote osteogenic differentiation of rBMSCs in both culture approaches and improve bone regeneration in osteoporosis zebrafish.

2. Materials and methods

2.1. Synthesis of SiO_2-CaO bioactive glass nanoparticles (BGNs)

Binary BGNs were synthesized using a modified Stöber method as described previously [29]. Briefly, solution A composed of 12 mL tetraethyl orthosilicate (TEOS, Sigma-Aldrich, USA) and 48 mL ethanol (VWR Chemicals, USA), was first mixed with solution B containing 18 mL ammonia (VWR Chemicals, USA), 33 mL ethanol and 100 mL deionized water for a 30 min reaction. Then, various amounts of calcium nitrate tetrahydrate (VWR Chemicals, USA) that matched the nominal compositions of designed BGNs (Table 1) were added to the above solution for Ca incorporation before a further 90 min reaction. After collection by centrifugation, washing and drying, the obtained particles underwent calcination conducted at 700 °C for 2 h using a heating rate of 2 °C/min. The harvested BGNs were denoted as 100S, 99S, 95S and 90S according to the designed concentrations of CaO in the composition. Table 1 shows the nominal compositions of BGNs and amounts of calcium nitrate tetrahydrate (CaN) added in the synthesis process.

2.2. Characterization of BGNs

The surface morphology of BGNs was visualized by employing field-emission scanning electron microscopy (FE-SEM, Auriga, Zeiss, Germany) under 3 kV accelerating voltage. The diameter of BGNs was determined according to SEM images using ImageJ (NIH, USA). The number of counted particles was >50. Hydrodynamic diameters and Zeta potential values of the particles were also measured in deionized water and α-minimum essential medium (α-MEM, Gibco, USA) at a concentration of 0.01 mg/mL using a Zetasizer Nano ZS instrument (Malvern Instruments, Malvern, UK). The samples were treated by a 4 mW HeNe laser (633 nm) with a light scattering detector positioned at 90°. The samples were analyzed at least in triplicate and each one consisted of 30 runs.

The concentrations of Si and Ca ions of deionized water, α-MEM and E3 (embryo) medium (5 mM NaCl, 0.17 mM KCl, 0.33 mM CaCl$_2$, 0.33 mM MgSO$_4$, 30 μL 1 % methylene blue) containing various BGNs at 1000 μg/mL for 24 h, shaken at 120 rpm, 37 °C were evaluated. Briefly, after 24 h soaking, the supernatant was collected and filtered with a 0.22 μm filter (Millipore, USA) before the measurement using inductively coupled plasma optical emission spectroscopy (ICP-OES, Aglient 7800, USA).

2.3. Isolation and culture of rBMSCs

rBMSCs were isolated from the femurs and tibias of 2-week-old Wistar rats. The animal experiments were conducted according to the protocols approved by the Experimental Animal Care Committee of Nanjing Medical University (IACUC-2111022). The bone marrow was flushed out of the bone cavity using α-MEM supplemented with 10 % fetal bovine serum (FBS, Vivacell, China) and 1 % penicillin-streptomycin (P/S, NCM Biotech, China). Cells were cultured under standard cell culture conditions of 5 % CO$_2$ at 37 °C. For each experiment, cells were initially seeded in the culture medium, with a change to the conditioned medium the following day. Culture medium was designed as the control.

2.4. Preparation of conditioned medium

To check the influence of BGNs on viability, proliferation, and osteogenic differentiation, rBMSCs and zebrafish larvae were exposed to BGNs in two different culture settings. Indirect culture approach: α-MEM and E3 (embryo) medium with or without BGNs was continuously shaken for 24 h at the speed of 120 rpm, 37 °C. After being filtered with a 0.22 μm filter (Millipore, USA), conditioned medium in the indirect culture approach was prepared for the following rBMSCs and zebrafish larvae culture. Direct culture approach: In this approach, α-MEM and E3 (embryo) medium with or without BGNs were dispersed ultrasonically and directly applied to rBMSCs and zebrafish larvae. The cell culture medium was refreshed every 3 days using the conditioned medium in cell studies and the embryo medium was refreshed daily in the Zebrafish experiment.

2.5. In vitro cytotoxicity

Cell viability in the presence of BGN extracts or BGNs was evaluated by the Cell Counting Kit-8 (CCK-8) assay (Dojindo Molecular Technologies, Japan) according to the manufacturer's protocol. In brief, rBMSCs were incubated with various concentrations of the dilution of conditioned medium individually (125, 250, 500, and 1000 μg/mL for indirect culture and 10, 100, and 1000 μg/mL for direct culture). The CCK-8 assay was performed on day 0, 1, 3 and 7 for indirect culture and day 0, 1, 4, and 7 for direct culture by adding 10 % CCK-8 solution. After 2 h incubation, the supernatants were measured at λ=450 nm on a microplate reader (SpectraMax M2e, Molecular Devices, USA). Based on the outcome of the CCK-8 assay, the highest BGN concentration that posed no noticeable cytotoxic effects was selected for the follow-up experiments.

Acridine Orange/Ethidium Bromide (AO/EB) double fluorescence staining kit (Beyotime, China) was used to evaluate the ratio of the number of dead and live rBMSCs. After being treated with a conditioned medium for 3 d, the slides were rinsed with PBS twice. 10 μL of dye mixture (AO solution: EB solution: AO/EB Dilution Buffer=1:1:8) was softly dropped onto slides that were observed immediately under a fluorescence microscope (DM4000, Leica, Germany).

For cytoskeleton staining, rBMSCs were fixed with 4 % paraformaldehyde (PFA, Biosharp, China) for 30 min at room temperature. Having been subjected to common immunocytochemical procedures, the cytoskeleton and nuclei were respectively stained with Acti-stain 488 phalloidin (PHDG1-A, Cytoskeleton, USA) in the dark for 1 h, and 4′,6-diamidino- 2-phenylindole (DAPI, Biosharp, China) for 5 min. The images were captured under a fluorescence microscope.

2.6. Alkaline phosphatase (ALP) and Alizarin red S (ARS) staining

ALP activity was assessed using BCIP/NBT ALP Color Development Kit (Beyotime, China) referred to the protocol. After culture for 7 d with conditioned medium, rBMSCs were fixed with 75 % ethanol for 15 min at 4 °C and dyed with the prepared BCIP/NBT solution for 15 min in the absence of light. After undergoing a gentle PBS washing, the images of stained cells were taken using a scanner (A3 Transparency Unit, EPSON, USA) and an inverted microscope (DFC2900, Leica, Germany).

After 14 d incubation with conditioned medium in osteogenic inductive conditions (the medium containing 100 mM l-ascorbic acid (Sigma, USA), 100 mM β-glycerophosphate (Sigma, USA), 1.8 mM potassium phosphate monobasic (Sigma, USA), and 10 nM dexamethasone (Sigma, USA), rBMSCs were fixed with 75 % ethanol for 15 min, followed by incubation with 1 % Alizarin Red S solution (Leagene, China) for 20 min. Finally, PBS was added to wash away superfluous dye and a scanner and a microscope were applied to examine the mineralized nodules. For quantitative analysis, 10 % cetylpyridinum chloride (Aladdin, China) in PBS was used to solubilize the red-stained nodules, and the absorbance values at 562 nm were measured.

2.7. Immunofluorescence

We also detected the expression of RUNX2 and OSX in rBMSCs after incubation with conditioned medium for 24 h by immunofluorescence staining. Cells were fixed by 4 % PFA for 20 min, incubated in 0.5 % Triton X-100 for 30 min for permeabilization, blocked for 30 min at 37 °C with goat serum, and then incubated with primary antibodies for RUNX2 (1:1000, Abcam, UK) and OSX (1:1000, Abcam, UK) overnight at 4 °C. Goat anti-mouse Alexa Fluor 488 (1:50, Beyotime, China) and goat anti-rabbit Cy3 (1:50, Beyotime, China) were employed as the secondary antibodies to combine the primary antibodies at 37 °C for 1 h. Finally, the nuclei was stained blue with DAPI, and fluorescent images were taken using a fluorescence microscope.

2.8. Zebrafish osteoporosis model

Zebrafish (Danio rerio) of wild-type Lon AB line, provided by the Model Animal Research Center of Nanjing University (Nanjing, China) were maintained at 28 °C on a 10:14 h dark: light cycle. The embryos were obtained from the copulation of adult zebrafish and incubated in deionized water for the first 72 h in an incubator at 28 °C. Then, the larvae were treated with BGNs in two approaches, i.e., the indirect and direct approaches. The larvae were divided randomly into 0.1 % DMSO (control group), 10 μM dexamethasone (Dex, model group), 10 μM Dex + BGNs extracts (1000 μg/mL) or BGNs (100 μg/mL) in E3 medium from 4 days post fertilization (dpf) to 8 dpf. The medium was refreshed daily to maintain the stability of the concentration of the component. All animal experiments were conducted according to the protocols approved by the Experimental Animal Care Committee of Nanjing Medical University.

2.9. Alizarin red staining of zebrafish larvae

To evaluate the level of bone mineralization, zebrafish larvae were stained with alizarin red as described previously [30]. In

Table 2
The sequence of primers used for qRT-PCR.

Genes	Forward (5′−3′)	Reverse (5′−3′)
Rat-Runx2	ATCCACAAGGACAGAGTC	TCAGATAAGAGGGGTAAG
Rat-Osx	AAGAAGCCCATTCACAGC	CTTGCCACAGAAAAGCCA
Rat-Alp	CCTGACTGACCCTTCCCT	AATCCTGCCTCCTTCCAC
Rat-Col1a1	CCAGACGCAGAAGTCATA	CAAAGTTTCCTCCAAGAC
Rat-Gapdh	GACATGCCGCCTGGAGAAAC	AGCCCAGGATGCCCTTTAGT
Dan-Runx2	GACTCCGACCTCACGACAA	CGTCCCGTCAGGAACATC
Dan-Osx	AAGAAACCTGTCCACAGCTG	GAGGCTTTACCGTACACCTT
Dan-Opn	CGCTCAGCAAGCAGTTCAGA	AGAATAGGAGGTGGCCGTTGA
Dan-Alp	AGAGAAGCGGCCTGATTACT	ACACCCATCCCATCTCCAAG
Dan-Col1a1	GAGTGATGGGTGCTATTGG	GGAATCCTCTGTCACCTCTA
Dan-β-actin	ACGAACGACCAACCTAAACTCT	TTAGACAACTACCTCCCTTTGC

brief, after being cultured for 8 dpf, zebrafish larvae were fixed with 4 % PFA overnight. Before staining, the pigment of the larvae was removed with the mixture of 2 % KOH and 3 % H_2O_2 at an equal ratio, and then alizarin red was utilized to mark the mineralized bone of the larvae. Finally, larvae were bleached again with 2 % KOH and 3 % H_2O_2 in a ratio of 1:1 to remove excess stain and observed using a microscope.

2.10. The mRNA expression of osteogenesis-related genes

Total RNA was extracted from rBMSCs and zebrafish larvae at 8 dpf using the FastPure® Cell/Tissue Total RNA Isolation Kit (Vazyme, China) according to the instructions. Then, cDNA was gained through reverse transcription using HiScript III RT Super-Mix for qPCR (Vazyme, China). Quantitative real-time PCR (qRT-PCR) was performed on QuantStudio 7 (ABI, USA) using ChamQ SYBR qPCR Master Mix (Q341−02, Vazyme, China). The classic $2^{-\Delta\Delta Ct}$ formula was adopted to calculate the relative expression. The primer sequences are listed in Table 2.

Runx2: Runt-related transcription factor 2; Osx: Osterix; Alp: Alkaline phosphatase; Col1a1: collagen I; Opn: Osteopontin; Gapdh: glyceraldehyde-3-phosphate dehydrogenase.

2.11. Endocytosis of BGNs

10 mg of BGNs were dispersed into 2 mL absolute ethanol (5% w/v), followed by being mixed with 100 μL 28 % ammonium hydroxide and 400 μL (3-aminopropyl) triethoxysilane (APTES, Macklin, China) on a shaker overnight at a speed of 200 rpm. Subsequently, 1 mg fluorescein 5 (6)-isothiocyanate (FITC, Macklin, China) was dissolved in 1% w/v BGNs ethanol suspension and stirred for 16 h to react completely. The FITC-conjugated BGNs were washed with absolute ethanol thrice and distilled water twice.

To confirm the internalization of BGNs into the cells and to identify the possible pathway of endocytosis, we pre-incubated rBMSCs with 23 μM of wortmannin (Macklin, China), 1 mM of amiloride hydrochloride hydrate (Aladdin, China), 30 μM of chlorpromazine hydrochloride (Aladdin, China), 3.7 mM of genistein (Aladdin, China) and 1 mM of methyl-β-cyclodextrin (Macklin, China) for 2 h before FITC-labeled BGNs treatment. After incubation with medium containing 100 μg/mL FITC-BGNs for 24 h, cells were fixed with 4 % PFA for cytoskeletal F-actin staining.

2.12. Western Blotting

Protein for Western Blotting was acquired from rBMSCs after culturing with BGNs for 72 h using RIPA lysis buffer (Beyotime, China) comprising protease inhibitors (PMSF, Beyotime, China). Equivalent proteins were added and separated by sodium dodecyl-sulfate polyacrylamide gel electrophoresis (SDS-PAGE), and further transferred to polyvinylidene difluoride (PVDF) membranes (Millipore, USA). After being blocked in 5 % skim milk solution (diluted with TBST buffer) for 2 h, the PVDF membranes were immersed in 1:100 diluted primary antibodies against RUNX2 (Cell Signaling Technology, USA), OSX (Abcam, USA) and GAPDH (Zsgb-bio, China) at 4 °C overnight. Following the thorough TBST wash, membranes were incubated with appropriate secondary antibodies (Goat anti-mouse, Proteintech, USA; Goat anti-rabbit, Proteintech, USA) for 1 h at room temperature. The immunoreactive bands were visualized with an Enhanced Chemiluminescent detection reagent (NCM Biotech, China).

2.13. Statistical analysis

All data were collected at least in three individual experiments and expressed as mean ± standard deviation (S.D.). Differences between each group were tested using one-way analysis of variance (ANOVA) and post hoc Tukey's test with a standard of $p < 0.05$ considered significant. Statistical analysis was performed by Graph-Pad PRISM 7.0a software.

3. Results

3.1. Characterization of BGNs

As displayed in SEM images (Fig. 1A), BGNs, regardless of CaO content, exhibited similar spherical morphology. The diameter ($n > 50$) of 100S, 99S, 95S and 90S were shown to be 158 ± 27, 133 ± 17, 114 ± 21 and 131 ± 15 nm, respectively, according to SEM images, which were in good agreement with the results published in our previous study [29]. In addition, we have confirmed that the actual compositions of 100S, 99S, 95S and 90S were the same as their nominal compositions [29]. We also evaluated the hydrodynamic diameter and zeta potential of BGNs (representative results are shown in Fig. 1B). Table 3 shows the measured hydrodynamic diameter and zeta potential values of various BGNs. The hydrodynamic diameters of 100S, 99S, 95S and 90S in H_2O were measured to be 148 ± 7, 181 ± 3, 139 ± 3 and 174 ± 11 nm, respectively, while their hydrodynamic diameters in α-MEM were 218 ± 11, 243 ± 5, 232 ± 16, and 246 ± 4 nm, respectively. As expected, the hydrodynamic diameters of BGNs were slightly larger than the diameters obtained in SEM images. However, the hydrodynamic diameters of BGNs in α-MEM were significantly larger than their diameters obtained in SEM images and measured in H_2O, probably due to the agglomeration of nanoparticles in culture medium [31]. All BGNs exhibited negative surface charge in both H_2O and in α-MEM, due to the presence of -OH groups on BGN surfaces in aqueous solution. The zeta potential values of all BGNs in H_2O were lower than −20 mV, suggesting their good stability in deionized water. These values of BGNs in α-MEM were higher than those in water, which suggested the reduced stability of BGNs in
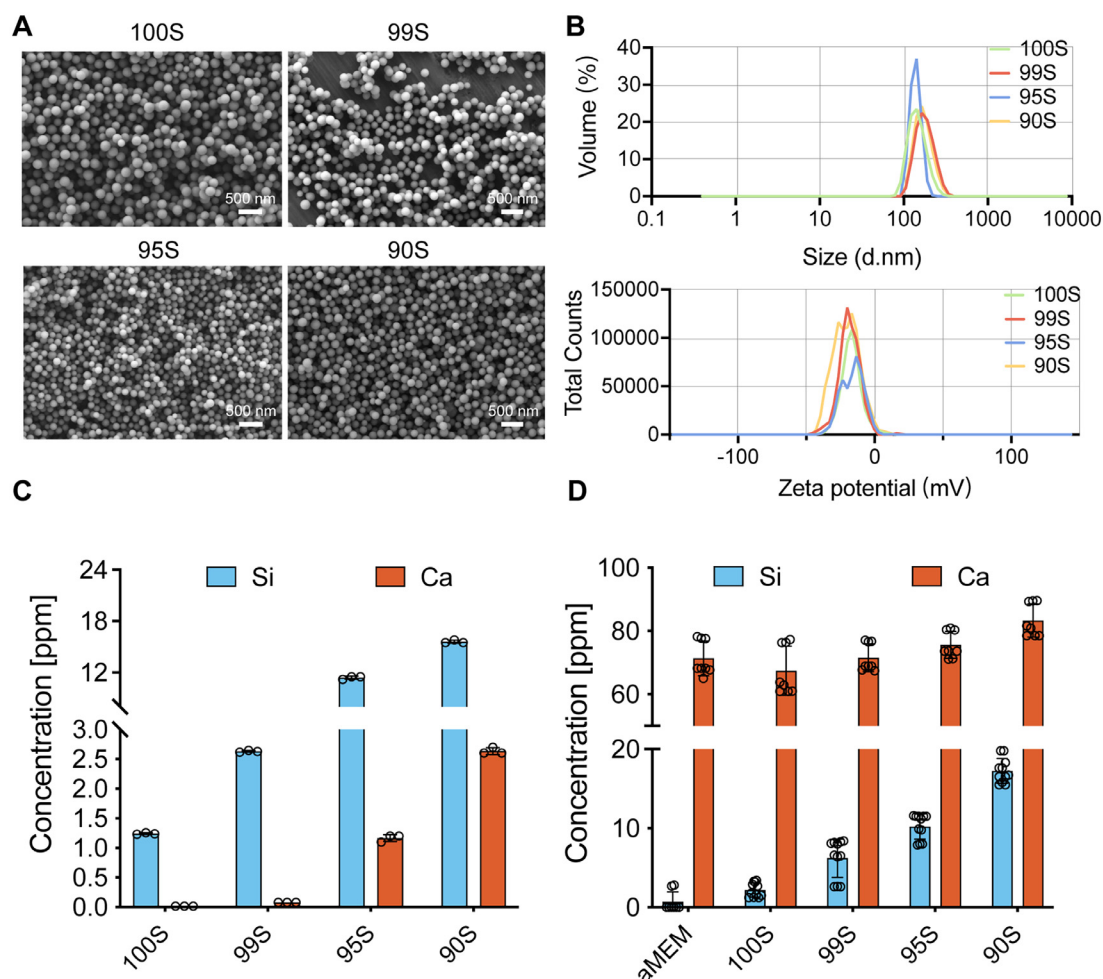
Fig. 1. (A) SEM images of 100S, 99S, 95S, and 90S. Scale bar = 500 nm. (B) Representative hydrodynamic diameter distribution and zeta potential of BGNs in H$_2$O. The concentrations of released Ca and Si ions from BGNs at 1000 μg/mL at 37 °C for 24 h in (C) deionized water and (D) α-MEM.

Table 3
Hydrodynamic diameter and Zeta potential values of various BGNs in H$_2$O and α-MEM.

BGNs	Hydrodynamic Diameter (nm)		Zeta Potential (mV)	
	H$_2$O	α-MEM	H$_2$O	α-MEM
100S	148 ± 7	218 ± 11	−26.1 ± 1.7	−9.6 ± 1.1
99S	181 ± 3	243 ± 5	−27.4 ± 1.4	−10.8 ± 1.5
95S	139 ± 3	232 ± 16	−26.4 ± 1.6	−8.6 ± 1.4
90S	174 ± 11	246 ± 4	−28.9 ± 0.9	−7.7 ± 1.3

α-MEM compared to water. However, BGNs still retained sufficient stability in the cell culture medium considering their zeta potential values [31].

Fig. 1C, D show the concentrations of Si and Ca ions released from BGNs after immersion in H$_2$O and α-MEM at 37 °C for 24 h, respectively. It has been evidenced that this type of binary BGNs could release Si and Ca ions in a sustained way [29]. Here we measured the ionic concentrations of various solutions containing BGNs in order to link the results with the effects of BGNs in indirect cell culture experiments. Fig. 1C shows the Si and Ca ion concentrations of BGNs after immersion in H$_2$O. As can be seen, the concertation of released Ca ions depended on the CaO content in BGNs. The nanoparticles with more CaO in the composition could release higher concentrations of Ca ions. 90S BGNs could release ~2.6 ppm Ca ions within 24 h in H$_2$O, while 95S and 99S showed a lower release level of Ca ions. As expected, 100S did not

release Ca ions. The release of Si ions displayed a conflict with the initial content of SiO$_2$ in BGNs. 90S and 95S exhibited higher Si ion release levels, while lower concentrations of Si ions were released from 99S and 100S. This phenomenon could be explained by the enhanced dissolution of BGNs with a higher CaO content [29]. It is known that CaO acts as a network modifier in silicate glasses, which can cause the Si-O-Si bonds break and introduce non-bridging oxygen, accelerating the degradation of silicate structure [32]. It is therefore understandable that the release of Si ions ascended with increasing CaO content. Generally, BGNs exhibited similar release behavior in α-MEM (Fig. 1D) and E3 medium (Fig. S2A), *i.e.*, BGNs with a higher amount of CaO could release more Si and Ca ions. After 24 h of immersion, the concentrations of Ca ions for 90S BGNs could reach ~ 83.3 ppm and ~16.2 ppm in α-MEM and E3 medium, respectively. It should be noted that both α-MEM and E3 medium intrinsically contain Ca ions. Therefore, more

Ca ions were detected in the medium. Our results confirmed the degradation and ion release behavior of BGNs in different aqueous medium.

3.2. In vitro *cytotoxicity of BGNs on rBMSCs in indirect culture*

According to ISO 10993-5, a decrease in cell viability up to 30 % is considered a toxic effect on cells, which was employed as the threshold value to assess the cytotoxicity of the particles. Compared to the control group (culture medium only), the tested gradient-diluted concentrations (125, 250, 500, and 1000 μg/mL) of the ionic dissolution products (BGN extracts) of four BGNs showed no significant impairment on rBMSCs viability. Notably, the cells cultivated in most of the diluted extract solutions of 95S-, 99S- and 100S-extracts presented enhanced proliferation by nearly 20 % on day 7. In comparison, the highest increase in viability by up to 30 % was induced by 95S-extract at 1000 μg/mL (Fig. 2A). Based on these results, the highest tested concentration of BGNs (1000 μg/mL) exhibiting no cytotoxic influence on rBMSCs was selected for further investigation in the indirect culture approach.

To further evaluate the cytotoxicity of BGN extracts at 1000 μg/mL, live/dead staining and cytoskeleton staining were conducted. All groups treated with BGN extracts exhibited similar live/dead staining images to the control group, in which most cells were alive (green). In contrast, a few dead cells (red) were observed (Fig. 2B). The cells incubated with BGN extracts maintained shape integrity and featured with polygonal morphology similar to their counterparts in the control group, suggesting the non-cytotoxicity of all samples exhibited against rBMSCs (Fig. 2C). The results confirmed that the ionic products of BGNs up to 1000 μg/mL concentration posed no negative influence on rBMSCs.

3.3. Osteogenic effects of BGNs on rBMSCs in indirect culture

ALP and ARS staining assay were employed to evaluate the early and late osteogenic differentiation of rBMSCs, respectively. All BGN extract groups significantly enhanced ALP activity compared to the control group (culture medium only). rBMSCs incubated in 95S-extract exhibited the highest ALP activity, while the other three BGN-extract groups showed similar ALP activity with each other (Fig. 3A, B). According to the ARS staining results, 90S-, 95S- and 99S-extracts led to a significant increase in ARS-positive mineral nodule formation compared to the control. In addition, the BGN extracts exhibited a Ca-dependent manner in ARS staining as the most calcium deposition was observed in the 90S-extract group (Fig. 3C, D). In parallel to the ALP and ARS staining, the expression of osteogenesis-related proteins (RUNX2 and OSX) was examined by immunofluorescence staining. Compared to the control, 95S and 90S extract groups exhibited higher immunofluorescence staining intensity of RUNX2 (Fig. 3E, F) and OSX (Fig. 3G, H), while 100S and 99S extract groups did not show significant differences in immunofluorescence staining intensity. In line with the results of immunofluorescence staining, qRT-PCR analysis demonstrated that the 90S-extract group induced significantly higher relative mRNA expression of all the tested osteogenic marker genes (Runx2, Col1a1, Osx, and Alp) than the control group (Fig. S1). 90S extract resulted in 1.82-fold upregulation of Runx2, 2.43-fold upregulation of Osx, 1.43-fold upregulation of Col1a1 and 1.92-fold upregulation of Alp, compared to the control. Other BGN-extracts also promoted the expression of osteogenic marker genes to different degrees compared to the control: 95S-extract upregulated the expression of Osx and Alp; 99S-extract upregulated the expression of Runx2, Osx, and Alp; 100S-extract upregulated the expression of Runx2, Col1a1, and Osx.

3.4. Cytotoxicity of BGNs on rBMSCs in direct culture

Fig. 4A shows the CCK-8 results of rBMSCs in culture with BGNs directly at 10, 100, and 1000 μg/mL. It is worth noting that 1000 μg/mL BGNs seemed to be tolerant to rBMSCs in the early incubation period (up to day 4), while on day 7, the viability of the cells turned to decline to below 70 %, revealing that the relatively high concentration (1000 μg/mL) of BGNs in direct culture might induce toxicity to cells. In comparison, at specific time points (primarily on day 4), the cell viability in 10 and 100 μg/mL groups was significantly increased compared to the control without BGNs treatment. 95S strongly increased cell viability by 44 % and 35 % at 10 and 100 μg/mL on day 4, while 90S increased cell viability by 27 % and 29 % at 10 and 100 μg/mL, respectively. Given the results shown above, we further investigated the impact of BGNs on rBMSCs in direct culture at the concentration of 100 μg/mL. The phalloidin staining pictured that cells incubated with 100 μg/mL BGNs exhibited a similar cell morphology of fully spread and rich pseudopodia extensions with the cells in control, suggesting the BGNs at 100 μg/mL did not harm the growth and adhesion of rBMSCs (Fig. 4B). Furthermore, the live/dead staining showed that most rBMSCs were alive in response to 100 μg/mL BGNs, and no extra cell apoptosis was caused compared to the control (Fig. 4C).

3.5. Osteogenic effects of BGNs on rBMSCs in direct culture

The osteogenic differentiation behaviors of rBMSCs in direct contact with BGNs were evaluated in terms of ALP activity, mineralization and immunofluorescence. ALP and ARS staining results demonstrated that stronger ALP staining and greater mineral nodule formation were intuitively detected in all BGN groups compared to the control (Fig. 5A, C). The quantitative analysis of ALP activity and ARS staining further revealed that 90S, 95S, and 99S induced osteogenic differentiation to a greater extent than the control group. Furthermore, the highest ALP activity was observed in the 95S group, followed by 90S and 99S groups, while the most calcium deposits were observed in the 90S group, followed by 95S, 99S, and 100S sequentially (Fig. 5A-D). The osteogenic commitment level of rBMSCs was also evaluated by immunofluorescence staining targeting at RUNX2 and OSX. As shown in Fig. 5E-H, the intracellular RUNX2 and OSX expression was enhanced in cells incubated with 90S and 95S. Compared to the control, a slight enhancement of RUNX2 and OSX staining intensity could be observed in the 99S and 100S groups. Of note, the trend of the increase of RUNX2 and OSX expression induced by BGNs was shown to rely on the CaO content of BGNs.

3.6. Bone regeneration of osteoporosis zebrafish induced by BGN extracts

The *in vivo* osteogenic effects induced by BGN extracts were evaluated in an osteoporosis zebrafish model. As shown in Fig. 6A, the presence of Dex seemed to increase the rate of malformation and death, while the introduction of BGN extracts did not cause extra malformation or death compared to the Dex group (treated with Dex only). Meanwhile, a reduction of pigment was observed in larvae treated with Dex, but the introduction of BGN extracts seemed to cause no significant change to a general view of larvae, including morphology, body length, and pigment (Fig. S2B-D).

Compared to the DMSO-treated control, Dex triggered decrease in the mRNA expression levels of all the tested osteogenic marker genes (0.34-fold change in Runx2, 0.34-fold change in Col1a1, 0.27-fold change in Osx, 0.46-fold change in Alp, and 0.29-fold change in Opn), suggesting the successful establishment of the osteoporosis zebrafish model. Conversely, compared to the Dex
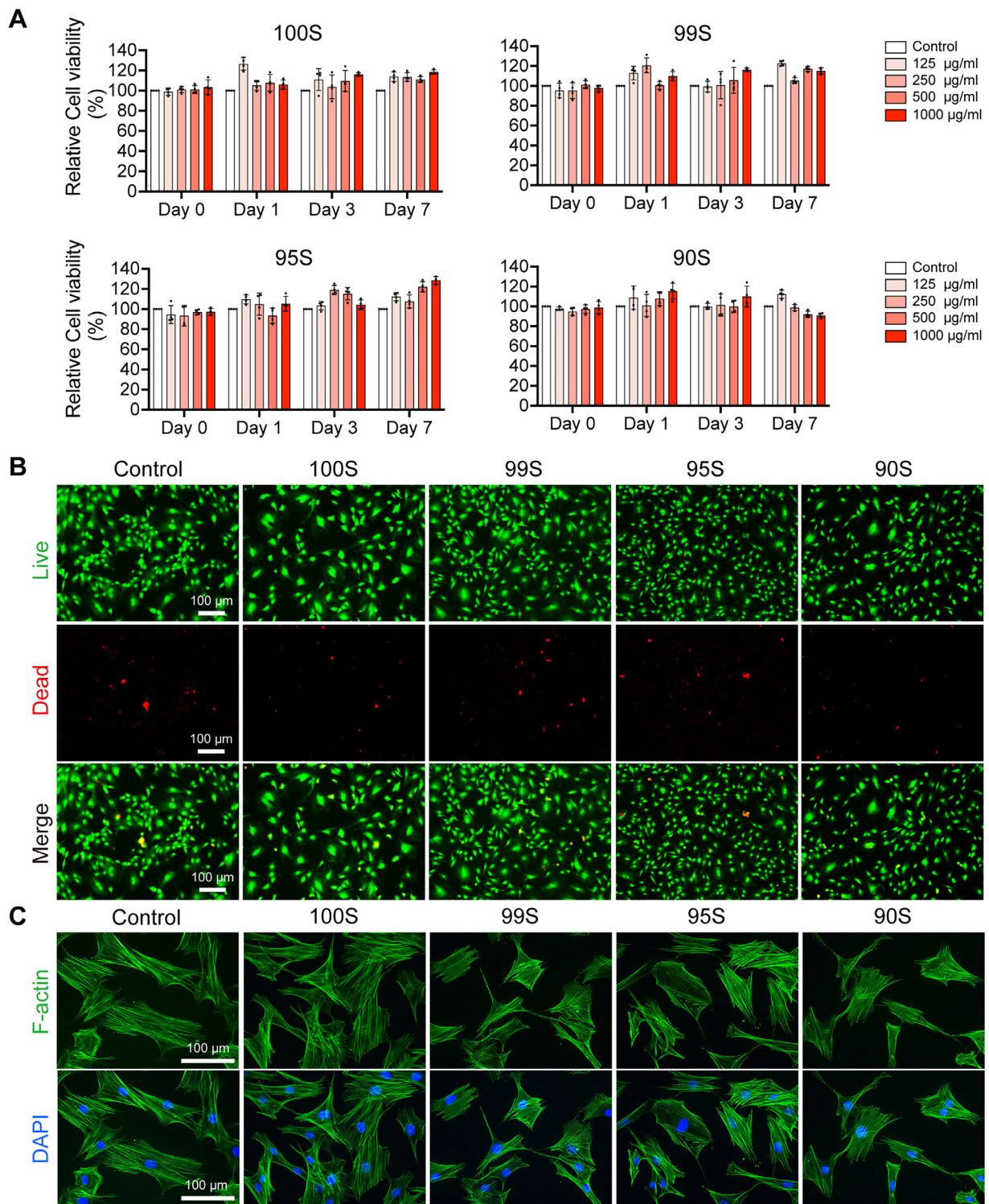
Fig. 2. *In vitro* cytotoxicity of BGNs on rBMSCs in indirect culture approach. (A) Cell viability of rBMSCs cultivated with BGN extracts (0, 125, 250, 500, and 1000 µg/mL) on day 0, 1, 3, and 7 obtained by using the CCK-8 assay. (B) Live/dead staining images of rBMSCs cultivated with BGN extracts (1000 µg/mL). Scale bar=100 µm. (C) Cytoskeletal morphology of rBMSCs in the presence of 1000 µg/mL BGN extracts, stained with FITC-phalloidin (green), and cell nuclei stained with DAPI (blue). Scale bar=100 µm. (For interpretation of the references to color in this figure legend, the reader is referred to the web version of this article.)

group, 90S-extract treatment relieved the downregulation expression of Runx2, Col1a1, Osx, Alp, and Opn with 0.59-, 0.52-, 0.37-, 0.58- and 0.66-fold changes respectively, relative to the control. The treatment of extracts from other BGNs could also relieve the downregulation expression of osteogenesis-related genes induced

by Dex (Fig. 6C). However, 90S-extract exerted the greatest effects on relieving the deteriorating osteogenic expression. The ARS staining showed that there was a decrease in the area and intensity of the cranial and vertebral bones stained with alizarin red in Dex-treated larvae compared to the control. Treatment with BGN-
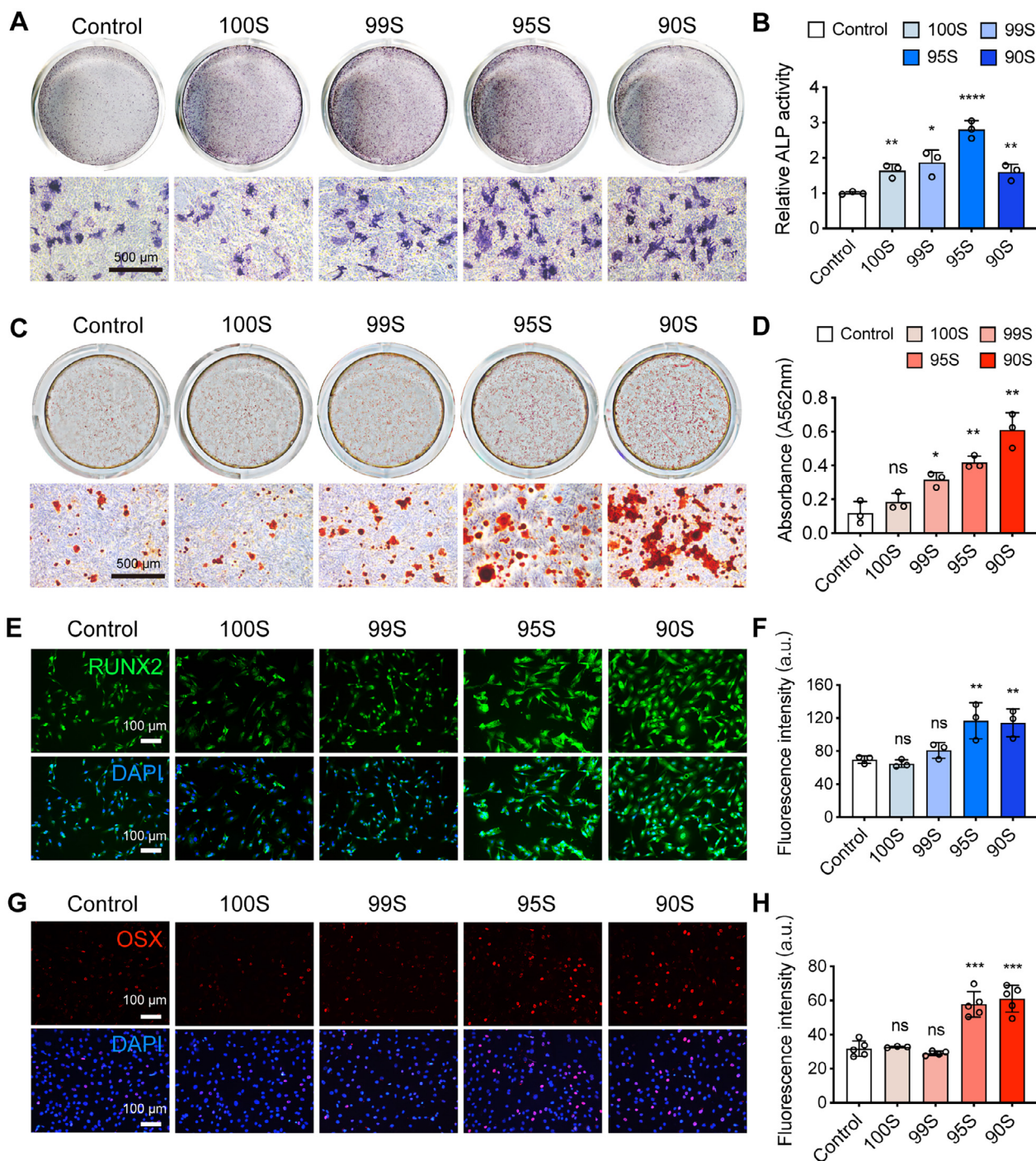
Fig. 3. Osteogenic capacity of BGNs on rBMSCs in indirect culture approach. (A) ALP staining after 7 d incubation of rBMSCs. Scale bar=500 μm. (B) Quantitative analysis of ALP staining. (C) ARS staining for calcified nodule formation after 14 d incubation of rBMSCs. Scale bar=500 μm. (D) Quantitative analysis of ARS staining. (E) Fluorescence staining of RUNX2 (green) in rBMSCs with nuclei stained blue. Scale bar=100 μm. (F) Quantitative analysis of fluorescence staining of RUNX2. (G) Fluorescence staining of OSX (red) in rBMSCs with nuclei stained blue. Scale bar=100 μm. (H) Quantitative analysis of fluorescence staining of OSX. ns, not significant, $*p < 0.05$, $**p < 0.01$, $***p < 0.001$, $**** p < 0.0001$. (For interpretation of the references to color in this figure legend, the reader is referred to the web version of this article.)

extracts (1000 μg/mL) relieved the Dex-induced deleterious effect on bone mineralization of partial skull (such as ceratohyal, branchiostegal ray 1, hyomandibular, parasphenoid, ectopterygoid) and trunk bones (such as vertebrae) in larval zebrafish. Consistent with the qRT-PCR results, the strongest relieved effects on osteoporosis zebrafish induced by BGN extracts occurred for 90S-extract with a 1.5-fold change of mineralization integrated optical density (IOD) compared to the Dex group (Fig. 6D, Fig. S2E).

3.7. Bone regeneration of osteoporosis zebrafish induced by BGNs in direct culture

In line with the results of indirect incubation, an increase in malformation and death rate was observed in groups treated with Dex. Larvae incubated in the medium containing BGNs (100 μg/mL) did not exhibit higher malformation and death rate compared to those incubated in the medium with Dex only (Fig. 7A). As shown
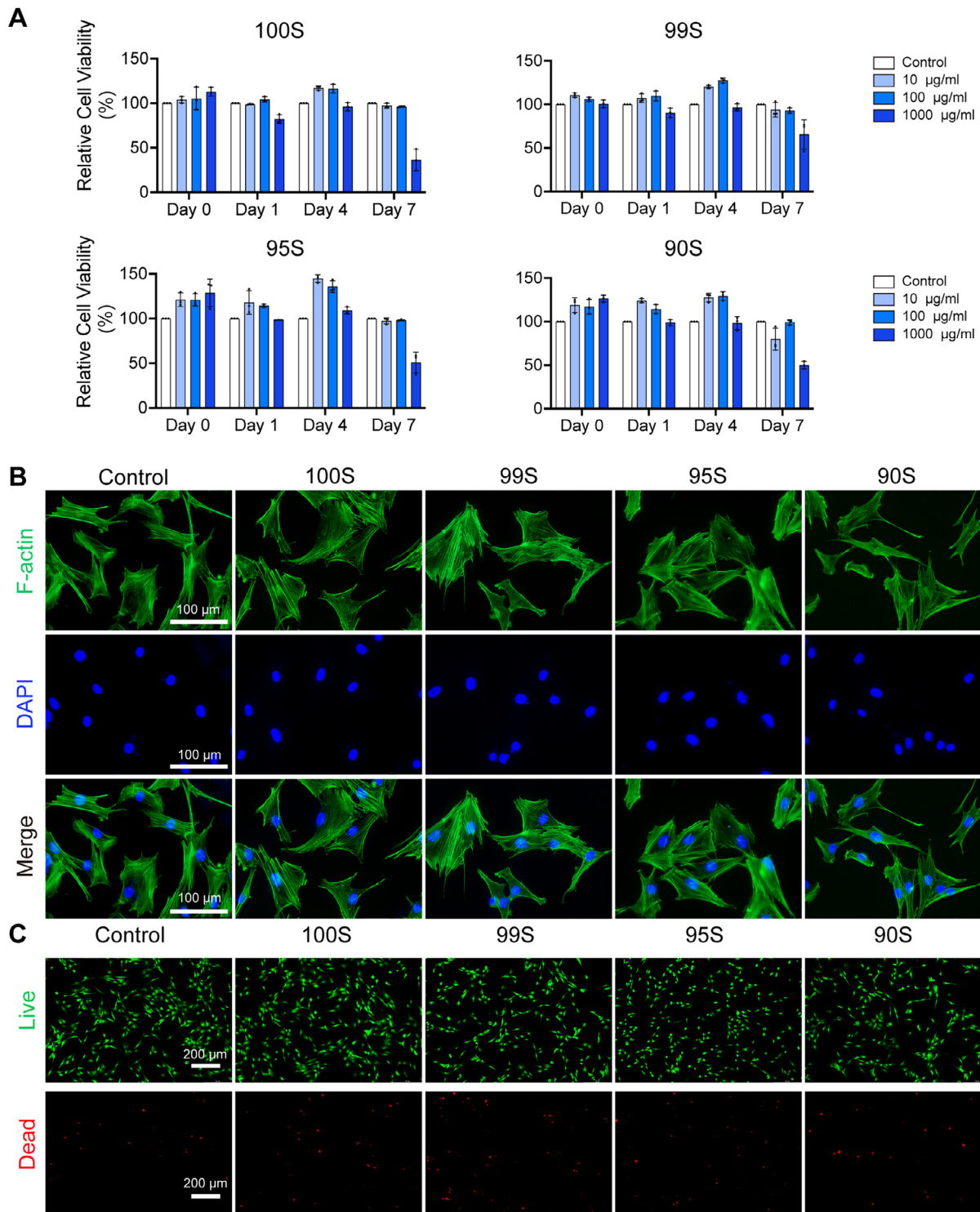
Fig. 4. Cytotoxicity of BGNs on rBMSCs in direct culture approach. (A) Cell viability of rBMSCs cultivated with BGN conditioned medium (0, 10, 100 and 1000 μg/mL) in the direct approach on day 0, 1, 4, and 7 by using the CCK-8 assay. (B) Cytoskeletal morphology of rBMSCs in the presence of 100 μg/mL BGNs, stained with phalloidin (green), and cell nuclei stained with DAPI (blue). Scale bar=100 μm. (C) Live/dead staining of rBMSCs in the presence of 100 μg/mL BGNs. Scale bar=200 μm. (For interpretation of the references to color in this figure legend, the reader is referred to the web version of this article.)

in Fig. S3A, C, the larvae treated with Dex at 4.5 dpf, presented a reduced level of melanin pigmentation, which was partly relieved by BGNs treatment. Subsequently, the gap of melanin pigment level between groups was narrowed at 8 dpf (Fig. S3C, E). The shape and body length of the larvae at 4.5 and 8 dpf in Dex- and BGNs-treated groups showed no significant difference com-

pared to the control (Fig. S3A, B, D). Consistent with the qRT-PCR results of indirect incubation, Dex exposure down-regulated Runx2 (0.51-fold), Col1a1 (0.07-fold), Osx (0.32-fold), Alp (0.61-fold), and Opn (0.13-fold) expression compared to the control group treated with DMSO (Fig. 7A). Notably, the 90S-treatment group significantly rescued the Dex-induced down-regulation of Runx2 (0.66-
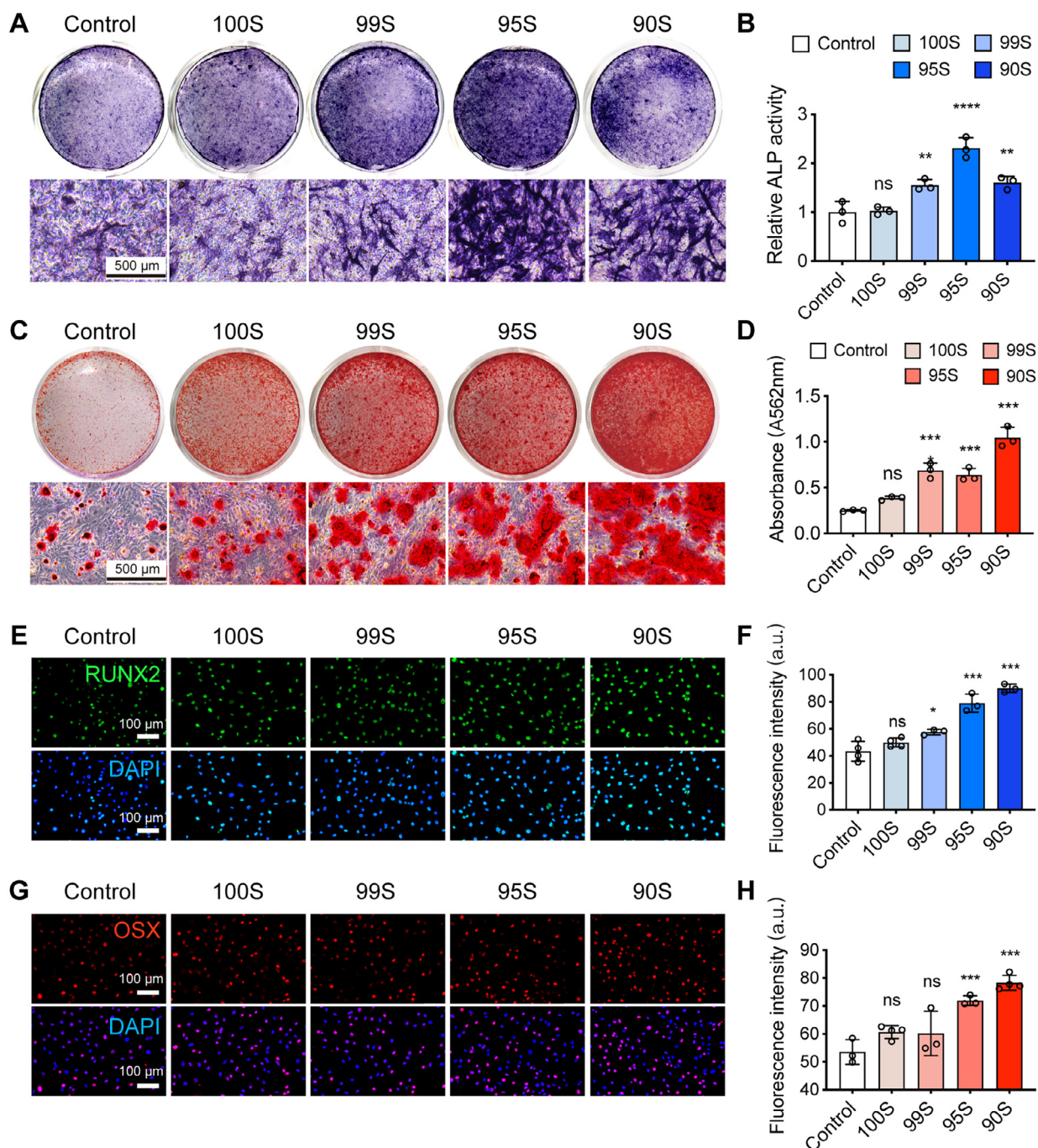
Fig. 5. Osteogenic effects of BGNs on rBMSCs in the direct culture approach. (A) ALP staining after 7 d incubation of rBMSCs with BGNs at 100 μg/mL. Scale bar=500 μm. (B) Quantitative analysis of ALP staining. (C) ARS staining following 14 d osteogenic incubation of rBMSCs with BGNs at 100 μg/mL. Scale bar=500 μm. (D) Quantitative analysis of ARS staining. (E) Fluorescence staining of RUNX2 (green) in rBMSCs with nuclei stained blue. Scale bar=100 μm. (F) Quantitative analysis of fluorescence staining of RUNX2. (G) Fluorescence staining of OSX (red) in rBMSCs with nuclei stained blue. Scale bar=100 μm. (H) Quantitative analysis of fluorescence staining of OSX. ns, not significant, $*p < 0.05$, $**p < 0.01$, $***p < 0.001$, $**** p < 0.0001$. (For interpretation of the references to color in this figure legend, the reader is referred to the web version of this article.)

fold), Col1a1 (0.13-fold), Osx (0.49-fold), Alp (0.82-fold), and Opn (0.21-fold) expression in relative to the control. The 95S- treatment group also increased the expression of the osteogenesis-related genes, though only Osx (1.25-fold change), Runx2 (1.27-fold change), and Opn (1.73-fold change) were significantly upregulated compared to the Dex-treated group. 99S and 100S seemed to have an insignificant impact on the expression of osteogenic marker genes (Fig. 7B–F) compared to the Dex-treated group. As

shown in Fig. 7G and Fig. S3F, the presence of BGNs attenuated the reduction induced by 10 μM Dex in the area and intensity of ARS staining in the cranial and vertebral bones of 8 dpf zebrafish larvae, especially in the 90S group, 2.29-fold greater in mineralization IOD than the Dex group was observed. 95S-treatment also induced bone regeneration in osteoporosis zebrafish with 1.84-fold changes of mineralization IOD compared to the Dex group.
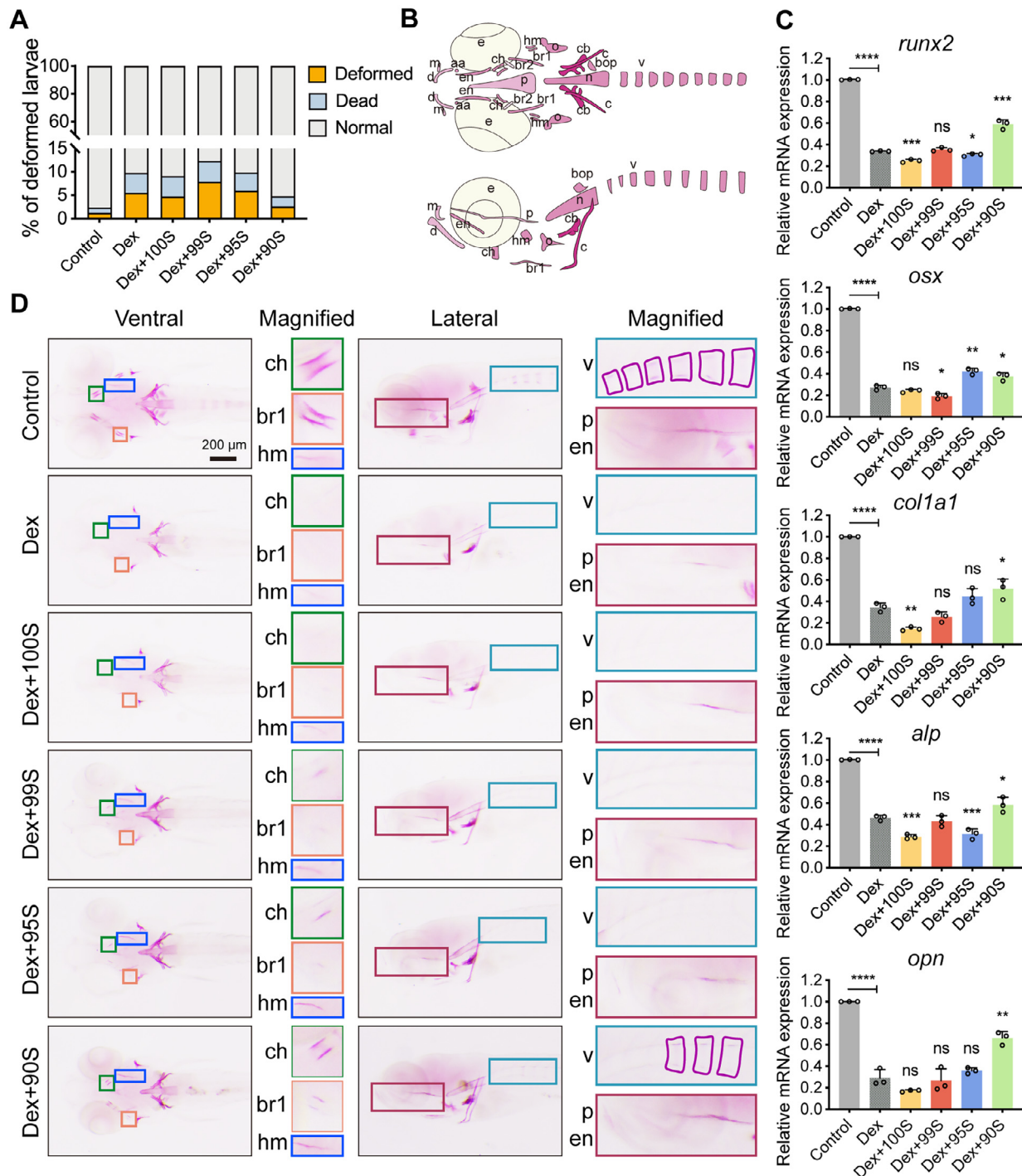
Fig. 6. Bone regeneration of osteoporosis zebrafish induced by BGN extracts. (A) Statistics of deformed zebrafish larvae ($n = 5$). (B) Schematic representation of the ventral (up) and lateral (down) view of bone structures in 8 dpf zebrafish. aa: anguloarticular, br1: branchiostegal ray1, en: ectopterygoid, m: maxilla, n: notochord, o: opercle, p: parasphenoid, br2: branchiostegal ray2, c: cleithrum, cb: ceratobranchial 5, ch: ceratohyal, d: dentary, hm: hyomandibular, v: vertebrae, bop: basioccipital articulatory process. (C) Osteogenesis-related gene expression of larvae detected by qRT-PCR. (D) ARS staining of bone elements in 8 dpf zebrafish larvae. Scale bar=200 μm. ns, not significant, $*p < 0.05$, $**p < 0.01$, $***p < 0.001$, $****p < 0.0001$.

3.8. Osteogenic transcription factors activation induced by internalization of BGNs

The cellular internalization of FITC-labeled BGNs was visualized by green fluorescence (Fig. 8). The fluorescent images depicted that rBMSCs maintained their morphologic integrity, indicating that the coculture of FITC-conjugated BGNs induced no significant negative effects on the cellular cytoskeleton structure. The enrichment of the FITC-conjugated BGNs in the cytoplasm of cells was observed, confirming the internalization of BGNs by rBMSCs. It is worth noting that the nanoparticles accumulated in the perinuclear zone of cells (Fig. 8A). To identify the potential endocytosis pathways inducing the internalization of BGNs, five specific endocytosis inhibitors, *i.e.*, wortmannin, amiloride hydrochloride hydrate, chlorpromazine hydrochloride, genistein and methyl-β-cyclodextrin, were employed to pre-treat rBMSCs. As can be seen,
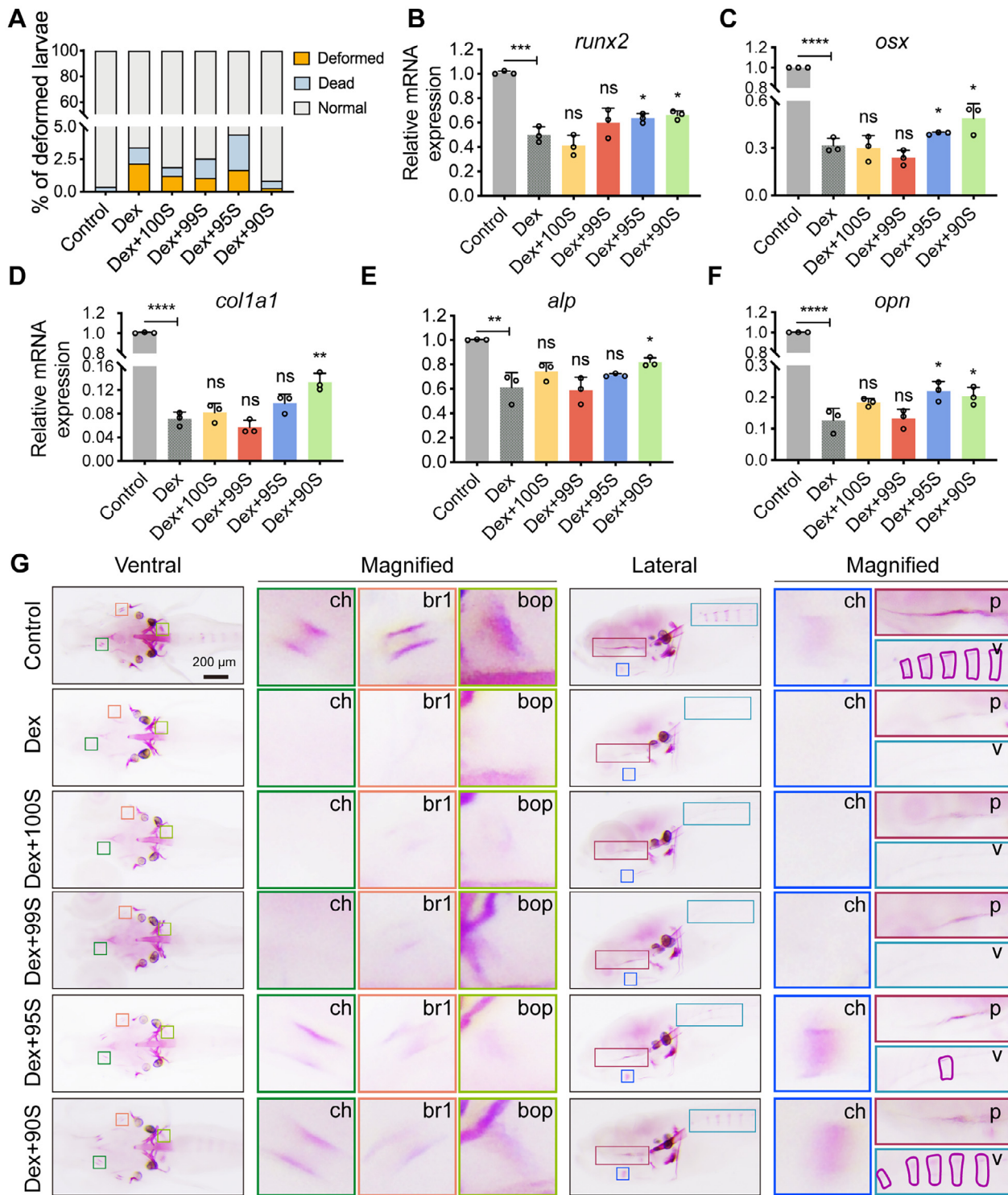
Fig. 7. Bone regeneration of osteoporosis zebrafish induced by BGNs in the direct culture approach. (A) Statistics of malformation in zebrafish larvae ($n = 5$). (B-F) Osteogenesis-related gene expression of larvae detected by qRT-PCR. (G) ARS staining of bone elements in 8 dpf zebrafish larvae. Scale bar=200 μm. ns, not significant, $^*p < 0.05$, $^{**}p < 0.01$, $^{***}p < 0.001$, $^{****}p < 0.0001$.

the uptake of nanoparticles was significantly suppressed by wortmannin and chlorpromazine in all BGN groups (Fig. 8B, C), while re-treatment with amiloride hydrochloride hydrate, genistein, and methyl-β-cyclodextrin did not appear to trigger a significant block on FITC–BGNs internalization by rBMSCs (Fig. 8C, Fig. S4A). The effect of BGNs on the protein synthesis of RUNX2 and OSX was investigated using western blotting. It was observed that the presence of BGNs upregulated the expression of RUNX2 and OSX in rBMSCs compared to the control (Fig. 8D). The upregulated expression of RUNX2 was positively correlated to the CaO content in BGNs and the highest OSX expression appeared in the 90S-treated group. To further study the effect of BGNs on osteogenic gene expression of rBMSCs, the qRT–PCR assay was employed and the results are shown in Fig. 8E. qRT–PCR analysis demonstrated
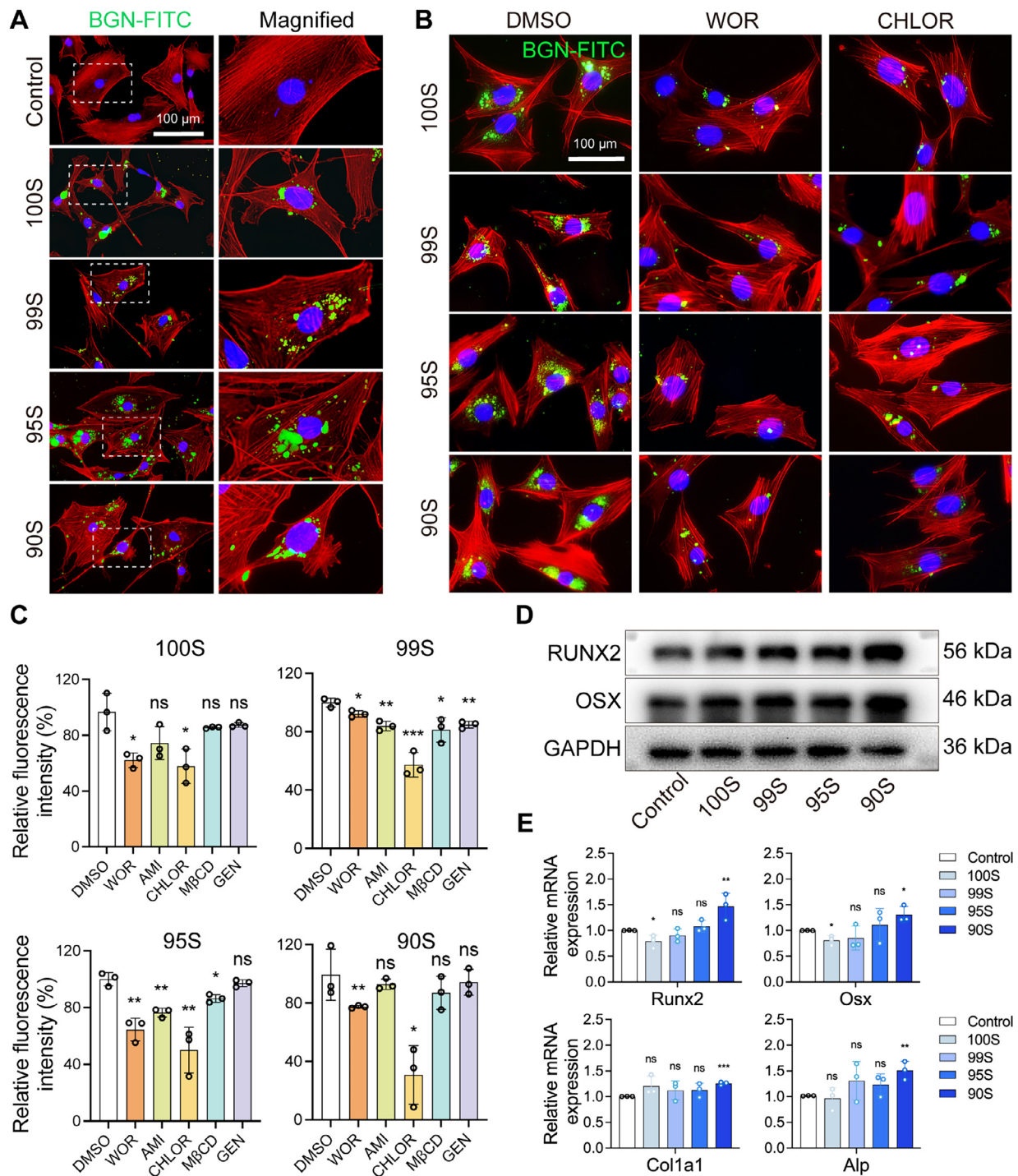
Fig. 8. Osteogenic transcription factors activation of rBMSCs induced by internalization of BGNs. (A) Fluorescent images visualizing internalization of FITC-BGNs by rBMSCs. Cytoskeleton stained red and nuclei stained blue. Scale bar=100 μm. (B) Fluorescent images of BGNs internalization by rBMSCs after 2 h pre-treatment with endocytosis inhibitors (Wortmannin and Chlorpromazine). Scale bar=100 μm. (C) Quantification of the inhibitory efficiency of BGNs uptake by endocytosis inhibitors. WOR (wortmannin), AMI (amiloride hydrochloride hydrate), CHLOR (chlorpromazine), MβCD (methyl-β-cyclodextrin), GEN (genistein). (D) The protein expression of RUNX2 and OSX in rBMSCs incubated in the direct culture approach (concentration at 100 μg/mL) confirmed by Western blotting. (E) Relative mRNA levels of osteogenesis-related genes (Runx2, Osx, Col1a1, Alp). ns, not significant, $*p < 0.05$, $**p < 0.01$, $***p < 0.001$. (For interpretation of the references to color in this figure legend, the reader is referred to the web version of this article.)

that the internalization of 90S induced significantly higher mRNA expression of all the tested osteogenic marker genes, with 1.47-, 1.36-, 1.23-, and 1.46-fold upregulation of Runx2, Osx, Col1a1 and Alp, respectively. However, the other three BGN groups seemed not to induce a significant increase in the expression of all tested osteogenesis-related genes.

Wortmannin has been employed as an inhibitor of micropinocy-tosis [33], or as an inhibitor of phagocytosis [34]. However, it has been reported that wortmannin can affect most endocytosis pathways, which lacks specificity [35]. Amiloride hydrochloride hydrate and chlorpromazine act as an inhibitor of macropinocyto-sis and clathrin-mediated endocytosis, respectively [36]. Methyl-

β-cyclodextrin and Genistein inhibit caveolae-mediated endocytosis/lipid rafts pathway [36]. In our study, a significant decrease in the internalization of all FITC-labeled BGNs by the cells treated with wortmannin and chlorpromazine was observed, while such a decrease was not significant in the groups treated with the other three inhibitors (Fig. 8B, C). Considering the poor specificity of wortmannin on internalization inhabitation (it affects most endocytosis pathways), we suppose the clathrin-mediated endocytosis inhibited by chlorpromazine, as the possible endocytosis pathway participating in the internalization of BGNs. However, inhibition of clathrin-dependent endocytosis by chlorpromazine did not result in complete suppression of uptake, which indicated that possibly different endocytosis pathways were involved in the internalization of BGNs. More specific methods should be used to determine the exact pathway guiding the internalization of BGNs, such as the knockout of key components in the endocytosis pathways or the expression of dominant-negative inhibitors in future studies [36].

4. Discussion

BGNs are multifunctional materials exhibiting osteogenic, angiogenic, and antibacterial properties, being increasingly investigated for various tissue regeneration scenarios, with a special focus on bone regeneration [37–39]. These beneficial biological properties of BGNs are mainly induced by released active ions. Among these biologically active ions, Ca ions play key roles in biomineralization and osteogenic activity that are important for the successful application of BGNs in bone regeneration. It should be pointed out that BGNs are usually applied as either rigid fillers of composites or delivery platforms of ion/drugs. In the former application, BGNs mainly affect cellular behavior through the released ions, while in the latter application, BGNs can directly interact with cells. Therefore, in this study, we developed a series of SiO_2-CaO BGNs with varying CaO contents from 0 to 10 mol% and investigated the influence of CaO content on *in vitro* and *in vivo* osteogenic activity of BGNs using indirect and direct culture approaches to mimic different application scenarios.

We first evaluated the influence of CaO content of BGNs on the osteoblastic differentiation of rBMSCs. Our results showed that osteoblastic differentiation of rBMSCs in both direct and indirect culture was promoted in the presence of BGNs. In the indirect culture approach, we used the extracts of BGNs at 1000 μg/mL in α-MEM for 24 h as the conditioned culture medium. During cell culture, the medium was refreshed every 3 days using the conditioned medium, a commonly applied method for the indirect culture approach [40]. Our results showed the Ca ion concentrations of various BGNs in α-MEM were in the range of 65–85 ppm, while the Si ion concentrations were in the range of 2–18 ppm (Fig. 1D). Hench et al. [41] have evidenced that bioactive ions could only induce osteostimulation effects when they are at a particular concentration range, for example, 15–30 ppm for Si ions and 60–90 ppm for Ca ions. The concentrations of Si and Ca ions of the conditioned medium in this study were in good agreement with the findings reported by Hench et al. In addition, we refreshed the conditioned medium every 3 days, which ensured the continuous stimulation of Si and Ca ions at proper concentration ranges. In the direct cell culture, BGNs can continuously release ions and exert intracellular effects on rBMSCs to stimulate osteoblastic differentiation. Generally, BGNs with a higher content of CaO could promote osteoblastic differentiation of rBMSCs to a greater extent as they could release more Si and Ca ions, which was consistent with the results reported previously [42]. Notably, the ALP activity of rBMSCs induced by 90S (Fig 3A, B and Fig 5A, B) was significantly lower than that caused by 95S, which was inconsistent with the results of ARS staining (Fig 3C, D and Fig 5C, D). This situation likely reflected the varying requirements for Ca ions in different osteogenic states

of rBMSCs. ARS staining illustrated the mineral depositions in the terminal differentiation stage, while ALP is one of the first phenotypical markers of osteoblasts and its activity subsequently declined with the onset of extracellular matrix deposition and mineralization [43]. The optimal concentrations of Ca ions for these osteogenic states are different. These results indicate that the release of bioactive ions from BGNs should be controlled spatiotemporally to achieve satisfactory outcomes as the beneficial biological effects of ions are concentration-dependent.

We have shown that BGNs could enhance osteogenic differentiation of rBMSCs in a Ca-content-dependent manner in both direct and indirect culture approaches. However, different concentrations of BGNs are required in the direct and indirect culture approaches to achieve promoted osteogenic differentiation of rBMSC compared to blank control (culture medium only). Our results showed that BGNs at 100 µg/mL in the direct culture could achieve comparable enhanced osteogenic differentiation of rBMSCs (compared to blank control) with BGNs at 1000 µg/mL in the indirect culture (Fig. 3 and Fig. 5). This difference could be explained by the ion release situation of BGNs. In the direct culture, BGNs could continually affect cells (by releasing ions) during cell culture. In addition, the internalization of BGNs enabled BGNs to affect cells intracellularly, which could stimulate the osteogenic activity of rBMSCs more effectively as the internalized nanoparticles mainly colocalized with lysosomes in a more compartmentalized and acidic environment [44]. We also investigated the mechanism of BGN promoting osteogenic differentiation in the direct approach. We found that BGNs could be internalized into rBMSCs around the nucleus via endocytosis and activated osteogenesis-related transcription factors, including RUNX2 and OSX to promote osteogenic differentiation (Fig. 8). These results highlight the fact that different therapeutic doses are available when BGNs of the same composition are applied in different ways.

Our *in vivo* data with the zebrafish osteoporosis model demonstrated that treatment with 1000 µg/mL BGNs-extracts hampered the Dex-induced deleterious effect on partial skull and trunk bone mineralization. Similarly, 100 µg/mL BGNs could also promote bone regeneration of the zebrafish osteoporosis model in the direct culture. To the best of our knowledge, this is the first study showing the bone regeneration effect of BGNs on osteoporotic zebrafish. Our results also demonstrated that either the dissolution products of BGNs or nanoparticles themselves could exert bone regeneration effects on zebrafish. In this context, the zebrafish model shows its great potential as a potent tool to screen osteogenesis stimulators *in vivo*. Particularly, our results validated the effects of the zebrafish model for evaluating the cytotoxicity and osteogenic activity of BGs under osteoporosis conditions. Zebrafish can readily absorb compounds from their aqueous environment. Therefore, dissolved compounds can be used to induce abnormal phenotypes of Zebrafish, such as the zebrafish osteoporosis model [45]. Dex is a synthetic glucocorticoid commonly used in medical treatments due to its anti-inflammatory and immunosuppressive properties. In the context of osteogenic differentiation, Dex is often included in cell culture medium to enhance the osteogenic differentiation of mesenchymal stem cells (MSCs) into osteoblasts. Dex can also be combined with biomaterials to promote osteogenic differentiation of cells [46]. However, Dex can also have deleterious effects on bone mineralization at excessive concentrations and induce osteoporosis. An osteoporosis animal model can thus be constructed relatively rapidly by using excess Dex [45]. Because of the ability to absorb environmental compounds, Zebrafish are also well suited for use in high-throughput, whole-organism, phenotypic drug/ion screens, designed to discover novel therapeutics [27]. The genetic similarity of zebrafish to humans, rapid development, regenerative capability, high fecundity, and experimental tractability make zebrafish ideal for investigating potential therapies for osteoporosis [45]. Ze-

brafish provide a powerful and versatile model system for studying the biological effects of BGs under osteoporosis. However, it should be noted that the zebrafish model also has limitations for evaluating the biological properties of biomaterials. The morphology and physiological properties of zebrafish bone have some differences from the human bone, which may compromise the translation of the findings in zebrafish to humans. For example, zebrafish do not have bone marrow that contains cells producing blood cells and platelets [47]. Nevertheless, zebrafish are increasingly used in bone disease and regeneration research, due to their convenience of genetic manipulation and *in vivo* imaging possibilities. The zebrafish model is expected to become more widely applied in the basic research and pre-clinical evaluation of BG-based medical devices.

5. Conclusions

In this study, we investigated the effects of binary SiO_2-CaO BGNs (CaO ranging from 0 to 10 mol%) on osteogenic differentiation of rBMSCs and *in vivo* bone regeneration in the zebrafish osteoporosis model. BGNs could stimulate osteogenic differentiation of rBMSCs by indirectly releasing active ions or directly interacting with rBMSCs. A higher CaO content facilitated the osteogenic differentiation of rBMSCs, bone regeneration, and rescue of the dexamethasone-induced osteoporosis in the zebrafish model. The internalization of BGNs by rBMSCs was probably achieved through clathrin-dependent endocytosis. BGNs exhibit great potential as either ion-releasing fillers or therapeutic nanoparticles for bone regeneration or osteogenesis treatment. The zebrafish osteoporosis model is shown to be a potent tool for evaluating the *in vivo* bone regeneration of bioactive materials.

Declaration of Competing Interest

The authors report no conflicts of interest in this work.

Acknowledgments

Supplementary materials

Supplementary material associated with this article can be found, in the online version, at doi:10.1016/j.actbio.2023.11.037.

References

[1] K. Zheng, B. Sui, K. Ilyas, A.R. Boccaccini, Porous bioactive glass micro- and nanospheres with controlled morphology: developments, properties and emerging biomedical applications, Mater. Horizons. 8 (2021) 300–335, doi:10.1039/d0mh01498b.

[2] M.N. Rahaman, D.E. Day, B.S. Bal, Q. Fu, S.B. Jung, L.F. Bonewald, A.P. Tomsia, Bioactive glass in tissue engineering, Acta Biomater. 7 (2011) 2355–2373, doi:10.1016/j.actbio.2011.03.016.

[3] M. Montazerian, E.D. Zanotto, Bioactive and inert dental glass-ceramics, J. Biomed. Mater. Res. Part A. 105 (2017) 619–639, doi:10.1002/jbm.a.35923.

[4] V. Miguez-Pacheco, L.L. Hench, A.R. Boccaccini, Bioactive glasses beyond bone and teeth: emerging applications in contact with soft tissues, Acta Biomater. 13 (2015) 1–15, doi:10.1016/j.actbio.2014.11.004.

[5] S. Naseri, W.C. Lepry, S.N. Nazhat, Bioactive glasses in wound healing: hope or hype? J. Mater. Chem. B. 5 (2017) 6167–6174, doi:10.1039/C7TB01221G.

[6] K. Zheng, A.R. Boccaccini, Sol-gel processing of bioactive glass nanoparticles : a review, Adv. Colloid Interface Sci. 249 (2017) 363–373, doi:10.1016/j.cis.2017.03.008.

[7] A.J. Leite, J.F. Mano, Biomedical applications of natural-based polymers combined with bioactive glass nanoparticles, J. Mater. Chem. B. 5 (2017) 4555–4568, doi:10.1039/c7tb00404d.

[8] A. Hoppe, N.S. Güldal, A.R. Boccaccini, A review of the biological response to ionic dissolution products from bioactive glasses and glass-ceramics, Biomaterials 32 (2011) 2757–2774, doi:10.1016/j.biomaterials.2011.01.004.

[9] O. Tsigkou, S. Labbaf, M.M. Stevens, A.E. Porter, J.R. Jones, Monodispersed bioactive glass submicron particles and their effect on bone marrow and adipose tissue-derived stem cells, Adv. Healthc. Mater. 3 (2014) 115–125, doi:10.1002/adhm.201300126.

[10] E. O'Neill, G. Awale, L. Daneshmandi, O. Umerah, K.W.H. Lo, The roles of ions on bone regeneration, Drug Discov. Today. 23 (2018) 879–890, doi:10.1016/j.drudis.2018.01.049.

[11] X. Kesse, C. Vichery, J.-M. Nedelec, Deeper insights into a bioactive glass nanoparticle synthesis protocol to control its morphology, dispersibility, and composition, ACS Omega 4 (2019) 5768–5775, doi:10.1021/acsomega.8b03598.

[12] X. Kesse, C. Vichery, A. Jacobs, S. Descamps, J.-M. Nedelec, Unravelling the impact of calcium content on the bioactivity of sol–gel-derived bioactive glass nanoparticles, ACS Appl. Bio Mater. 3 (2020) 1312–1320, doi:10.1021/acsabm.0c00036.

[13] K. Zheng, N. Taccardi, A.M. Beltran, B. Sui, T. Zhou, V.R.R. Marthala, M. Hartmann, A.R. Boccaccini, Timing of calcium nitrate addition affects morphology, dispersity and composition of bioactive glass nanoparticles, RSC Adv. 6 (2016) 95101–95111, doi:10.1039/C6RA05548F.

[14] A.A. El-Rashidy, J.A. Roether, L. Harhaus, U. Kneser, A.R. Boccaccini, Regenerating bone with bioactive glass scaffolds: a review of *in vivo* studies in bone defect models, Acta Biomater. 62 (2017) 1–28, doi:10.1016/j.actbio.2017.08.030.

[15] S. Vimalraj, R. Yuvashree, G. Hariprabu, R. Subramanian, P. Murali, D.N. Veeraiyan, L. Thangavelu, Zebrafish as a potential biomaterial testing platform for bone tissue engineering application: a special note on chitosan based bioactive materials, Int. J. Biol. Macromol. 175 (2021) 379–395, doi:10.1016/j.ijbiomac.2021.02.005.

[16] J.W. Bek, C. Shochat, A. De Clercq, H. De Saffel, A. Boel, J. Metz, F. Rodenburg, D. Karasik, A. Willaert, P.J. Coucke, Lrp5 mutant and crispant zebrafish faithfully model human osteoporosis, establishing the zebrafish as a platform for CRISPR-based functional screening of osteoporosis candidate genes, J. Bone Miner. Res. 36 (2021) 1749–1764, doi:10.1002/jbmr.4327.

[17] N. Li, K. Felber, P. Elks, P. Croucher, H.H. Roehl, Tracking gene expression during zebrafish osteoblast differentiation, Dev. Dyn. 238 (2009) 459–466, doi:10.1002/dvdy.21838.

[18] M.T. Valenti, G. Marchetto, M. Mottes, L.D. Carbonare, Zebrafish: a suitable tool for the study of cell signaling in bone, Cells 9 (2020) 1–14, doi:10.3390/cells9081911.

[19] T.S.P. Rothenbücher, J. Ledin, D. Gibbs, H. Engqvist, C. Persson, G. Hulsart-Billström, Zebrafish embryo as a replacement model for initial biocompatibility studies of biomaterials and drug delivery systems, Acta Biomater. 100 (2019) 235–243, doi:10.1016/j.actbio.2019.09.038.

[20] J.M. Lane, L. Russell, S.N. Khan, in Osteoporosis, Clin. Orthop. Relat. Res. (2000) 139–150, doi:10.1097/00003086-200003000-00016.

[21] M.A. Clynes, N.C. Harvey, E.M. Curtis, N.R. Fuggle, E.M. Dennison, C. Cooper, The epidemiology of osteoporosis, Br. Med. Bull. 133 (2020) 105–117, doi:10.1093/bmb/ldaa005.

[22] P. Naruphontjirakul, O. Tsigkou, S. Li, A.E. Porter, J.R. Jones, Human mesenchymal stem cells differentiate into an osteogenic lineage in presence of strontium containing bioactive glass nanoparticles, Acta Biomater. 90 (2019) 373–392, doi:10.1016/j.actbio.2019.03.038.

[23] S. Kargozar, N. Lotfibakhshaiesh, J. Ai, M. Mozafari, P. Brouki Milan, S. Hamzehlou, M. Barati, F. Baino, R.G. Hill, M.T. Joghataei, Strontium- and cobalt-substituted bioactive glasses seeded with human umbilical cord perivascular cells to promote bone regeneration via enhanced osteogenic and angiogenic activities, Acta Biomater. 58 (2017) 502–514, doi:10.1016/j.actbio.2017.06.021.

[24] P.P. Lelovas, T.T. Xanthos, S.E. Thorma, G.P. Lyritis, I.A. Dontas, The laboratory rat as an animal model for osteoporosis research, Comp. Med. 58 (2008) 424–430.

[25] J.T. Rosa, V. Laizé, P.J. Gavaia, M.L. Cancela, Fish models of induced osteoporosis, Front. Cell Dev. Biol. 9 (2021) 672424, doi:10.3389/fcell.2021.672424.

[26] S. Font Tellado, J.A. Delgado, S.P.P. Poh, W. Zhang, M. Garcia-Valles, S. Martinez, A. Gorustovich, L. Morejon, M. Van Griensven, E.R. Balmayor, Phosphorous pentoxide-free bioactive glass exhibits dose-dependent angiogenic and osteogenic capacities which are retained in glass polymeric composite scaffolds, Biomater. Sci. 9 (2021) 7876–7894, doi:10.1039/d1bm01311d.

[27] M. Montazerolghaem, L. Nyström, H. Engqvist, M.K. Ott, Zebrafish: a possible tool to evaluate bioactive ions, Acta Biomater. 19 (2015) 10–14, doi:10.1016/j.actbio.2015.03.010.

[28] L.B. Romero-Sánchez, M. Marí-Beffa, P. Carrillo, M.Á. Medina, A. Díaz-Cuenca, Copper-containing mesoporous bioactive glass promotes angiogenesis in an *in vivo* zebrafish model, Acta Biomater. 68 (2018) 272–285, doi:10.1016/j.actbio.2017.12.032.

[29] M. Kapp, C. Li, Z. Xu, A.R. Boccaccini, K. Zheng, Protein adsorption on SiO2-CaO bioactive glass nanoparticles with controllable Ca content, Nanomaterials 11 (2021) 561.

[30] M.B. Walker, C.B. Kimmel, A two-color acid-free cartilage and bone stain for zebrafish larvae, Biotech. Histochem. 82 (2007) 23–28, doi:10.1080/10520290701333558.

[31] C. Graf, Q. Gao, I. Schütz, C.N. Noufele, W. Ruan, U. Posselt, E. Korotianskiy, D. Nordmeyer, F. Rancan, S. Hadam, A. Vogt, J. Lademann, V. Haucke, E. Rühl, Surface functionalization of silica nanoparticles supports colloidal stability in physiological media and facilitates internalization in cells, Langmuir 28 (2012) 7598–7613, doi:10.1021/la204913t.

[32] X. Li, L. Zhang, X. Dong, J. Liang, J. Shi, Preparation of mesoporous calcium doped silica spheres with narrow size dispersion and their drug loading and degradation behavior, Microporous Mesoporous Mater. 102 (2007) 151–158, doi:10.1016/j.micromeso.2006.12.048.

[33] V. Sokolova, D. Kozlova, T. Knuschke, J. Buer, A.M. Westendorf, M. Epple, Mechanism of the uptake of cationic and anionic calcium phosphate nanoparticles by cells, Acta Biomater. 9 (2013) 7527–7535.

[34] P. Naruphontjirakul, A.E. Porter, J.R. Jones, *In vitro* osteogenesis by intracellular uptake of strontium containing bioactive glass nanoparticles, Acta Biomater. 66 (2018) 67–80, doi:10.1016/j.actbio.2017.11.008.

[35] M.S. de Almeida, E. Susnik, B. Drasler, P. Taladriz-Blanco, A. Petri-Fink, B. Rothen-Rutishauser, Understanding nanoparticle endocytosis to improve targeting strategies in nanomedicine, Chem. Soc. Rev. 50 (2021) 5397–5434.

[36] J.J. Rennick, A.P.R. Johnston, R.G. Parton, Key principles and methods for studying the endocytosis of biological and nanoparticle therapeutics, Nat. Nanotechnol. 16 (2021) 266–276, doi:10.1038/s41565-021-00858-8.

[37] T. Tian, W. Xie, W. Gao, G. Wang, L. Zeng, G. Miao, B. Lei, Z. Lin, X. Chen, Micro-nano bioactive glass particles incorporated porous scaffold for promoting osteogenesis and angiogenesis *in vitro*, Front. Chem. 7 (2019) 1–11, doi:10.3389/fchem.2019.00186.

[38] W. Xie, X. Fu, F. Tang, Y. Mo, J. Cheng, H. Wang, X. Chen, Dose-dependent modulation effects of bioactive glass particles on macrophages and diabetic wound healing, J. Mater. Chem. B 7 (2019) 940–952, doi:10.1039/c8tb02938e.

[39] J. Zheng, F. Zhao, W. Zhang, Y. Mo, L. Zeng, X. Li, X. Chen, Sequentially-crosslinked biomimetic bioactive glass/gelatin methacryloyl composites hydrogels for bone regeneration, Mater. Sci. Eng. C 89 (2018) 119–127, doi:10.1016/j.msec.2018.03.029.

[40] P. Sutthavas, M. Schumacher, K. Zheng, P. Habibović, A.R. Boccaccini, S. van Rijt, Zn-loaded and calcium phosphate-coated degradable silica nanoparticles can effectively promote osteogenesis in human mesenchymal stem cells, Nanomaterials 12 (2022) 2918, doi:10.3390/nano12172918.

[41] L.L. Hench, Genetic design of bioactive glass, J. Eur. Ceram. Soc. 29 (2009) 1257–1265, doi:10.1016/j.jeurceramsoc.2008.08.002.

[42] S. Maeno, Y. Niki, H. Matsumoto, H. Morioka, T. Yatabe, A. Funayama, Y. Toyama, T. Taguchi, J. Tanaka, The effect of calcium ion concentration on osteoblast viability, proliferation and differentiation in monolayer and 3D culture, Biomaterials 26 (2005) 4847–4855, doi:10.1016/j.biomaterials.2005.01.006.

[43] O. Tsigkou, J.R. Jones, J.M. Polak, M.M. Stevens, Differentiation of fetal osteoblasts and formation of mineralized bone nodules by 45S5 Bioglass® conditioned medium in the absence of osteogenic supplements, Biomaterials 30 (2009) 3542–3550, doi:10.1016/j.biomaterials.2009.03.019.

[44] N. Hassani Besheli, J. Verbakel, M. Hosseini, L. Andrée, B. Joosten, X.F. Walboomers, A. Cambi, F. Yang, S.C.G. Leeuwenburgh, Cellular uptake of modified mesoporous bioactive glass nanoparticles for effective intracellular delivery of therapeutic agents, Int. J. Nanomed. 18 (2023) 1599–1612, doi:10.2147/IJN.S397297.

[45] D.J.M. Bergen, E. Kague, C.L. Hammond, Zebrafish as an emerging model for osteoporosis: a primary testing platform for screening new osteo-active compounds, Front. Endocrinol. 10 (2019) 6, doi:10.3389/fendo.2019.00006.

[46] N. Aslankoohi, S. Lin, K. Mequanint, Bioactive fluorescent hybrid microparticles as a stand-alone osteogenic differentiation inducer, Mater. Today Bio. 13 (2022) 100187, doi:10.1016/j.mtbio.2021.100187.

[47] K. Dietrich, I.A.K. Fiedler, A. Kurzyukova, A.C. López-Delgado, L.M. McGowan, K. Geurtzen, C.L. Hammond, B. Busse, F. Knopf, Skeletal biology and disease modeling in zebrafish, J. Bone Miner. Res. 36 (2021) 436–458, doi:10.1002/jbmr.4256.